

# Vortex Lattices in Stripe Domains of Ferromagnet/Superconductor Bilayer

Serkan Erdin

Department of Physics, Northern Illinois University, DeKalb, IL, 60115  
& Advanced Photon Source, Argonne National Laboratory,  
9700 South Cass Avenue, Argonne, IL, 60439

The continuum theory of domain structures in ferromagnetic/superconducting bilayers fails when the equilibrium domain size becomes comparable with effective penetration depth  $\Lambda$ . Instead, a lattice of discrete vortices must be considered. Here, we report our results on the discrete vortex lattices in stripe domain structures of ferromagnetic/superconducting bilayers. The vortices are assumed to be situated periodically on chains in stripe domains. We study the configurations containing up to three chains per domain, and calculate their equilibrium energies, equilibrium domain size and vortex positions through a method based on London-Maxwell equations. In equilibrium, the vortices in the neighbor domains are half-way shifted while they are next to each other in the same domain. Additionally, more vortex chains per domain appear spontaneously depending on magnetization and domain wall energy.

PACS Number(s): 74.25.Dw, 74.25.Ha, 74.25.Qt, 74.78.-w

## I. INTRODUCTION

Heterostructures made of superconducting (SC) and ferromagnetic (FM) pieces not only give rich physical effects that are not observed in individual subsystems, but also offer new devices that can be tuned by weak magnetic fields [1,2]. One of the realizations of such heterostructures is ferromagnetic/superconducting bilayer (FSB). Earlier Lyuksyutov and Pokrovsky noticed [3,4] that in a bilayer consisting of homogeneous SC and FM films with the magnetization normal to the plane, SC vortices occur spontaneously in the ground state, even though the magnet does not generate a magnetic field in the SC film.

In previous work, we presented a theory of such vortex-generation instability and the resulting vortex structures [5]. We showed that due to this instability, domains with alternating magnetization and vortex directions occur in FSB. In that study, we treated these domain structures in the continuum regime in which the domain size is much larger than the effective penetration depth, which is defined to be  $\Lambda = \lambda^2/d_{sc}$ , where the London penetration depth  $\lambda$  is much larger than the thickness of superconducting film  $d_{sc}$  [6]. Under the continuum approximation, we found that the energy of stripe phase was minimal. The equilibrium domain size and the equilibrium energy for the stripe structure was found as [5]

$$L_{eq}^{(str)} = \frac{\Lambda}{4} \exp\left(\frac{\varepsilon_{dw}}{4\tilde{m}^2} - C + 1\right), \quad (1)$$

$$U_{eq}^{(str)} = -\frac{16\tilde{m}^2\mathcal{A}}{\Lambda} \exp\left(-\frac{\varepsilon_{dw}}{4\tilde{m}^2} + C - 1\right). \quad (2)$$

where  $\tilde{m} = m - \varepsilon_v/\phi_0$ ,  $\varepsilon_v = (\phi_0^2/16\pi^2\Lambda) \ln(\Lambda/\xi)$  is self-energy of a vortex,  $\varepsilon_{dw}$  is domain wall energy per domain wall length,  $\mathcal{A}$  is the domain's area and  $C \sim 0.577$  is the Euler-Mascheroni constant. If  $\varepsilon_{dw} \leq 4\tilde{m}^2$ , the continuum approximation becomes invalid, since  $L_{eq}$  becomes on the order of or less than  $\Lambda$  (see Eq.(1)). However, it can be recovered by considering the discrete lattice of vortices instead.

In this paper, we study the discrete lattice of vortices in stripe domain structures in FSB via a method based on London-Maxwell equations, which is developed elsewhere [7]. The extension of the method to periodic systems is also introduced for the case of square magnetic dot arrays on a SC film [8]. Here we adapt it for the discrete vortex lattices in SC/FM bilayers. In doing so, we assume that vortices and antivortices sit periodically on chains in the alternating domains of magnetization and vorticity. The problems we consider here are; i) how the vortices and the antivortices are positioned on the chains; ii) how the equilibrium domain size changes, depending on the magnetization and the magnetic domain wall energy in the presence of the vortices; iii) if the spontaneous appearance of domains structures with different number of vortex chains is possible. In order to solve these problems, we first propose five different configurations of the vortex and the antivortex chains, in which at most two chains per stripe is considered. Next, we calculate their equilibrium energies by means of numerical methods and find the most favorable case among them. Our calculations show that in equilibrium structure, vortex chains are half shifted in the adjacent domain while they are next to each other in the same domains. Inspired from this result, similar configuration for three vortex chains per domain is considered, and its equilibrium energy is

calculated for various values of magnetization and domain wall energy. Comparison of equilibrium energies of cases with one, two and three chains per domains shows that at lower values of magnetization and domain wall energy case with two chains is favorable whereas, three chain cases wins at higher values of magnetization and domain wall energy. Additionally, single chain case does not win over the ones with two and three chains per domain under any circumstances.

The outline of this paper is as follows: In the following section, we present the method for discrete case and its application to configurations with a single and double vortex chains per domain. In the third section, we briefly present our results on the proposed five configurations. The fourth section is devoted to the study of the case with three chains per domain. The last section consists of the conclusions and discussion. In the appendix, we give the details of the methods and mathematical tricks in series calculations.

## II. METHOD

In this section, we introduce a method based on the treatment of vortices in the discrete lattice. We study the lattices of discrete vortices only in the stripe phase. In the continuum approximation, it is found that the vortex density increases at the closer distances to the magnetic domain walls. Based on this fact and the symmetry of the stripe domain structure, it is reasonable to consider that the vortices and antivortices form periodic structures on straight chains along the  $y$  direction. Even though it is not clear how many chains are associated with each domain, we can still make progress toward understanding discrete vortex lattices. To this end, five stripe domain configurations in which vortices are situated periodically on chains are proposed. From this point on, the configurations with  $N$  vortex chains per stripe domain are labeled as  $N$  state.

In two of proposed cases, there is one chain per stripe ( $N = 1$  states), located in the middle of the domain. In this case, two configurations of vortex lattice are possible; first, the vortices and the antivortices in a neighboring domains are alongside to one another (see Fig. 1(a)), second, they are shifted by half period  $b/2$  along the  $y$  direction, where  $b$  is the distance between two nearest vortices on the chain (see Fig. 1(b)).

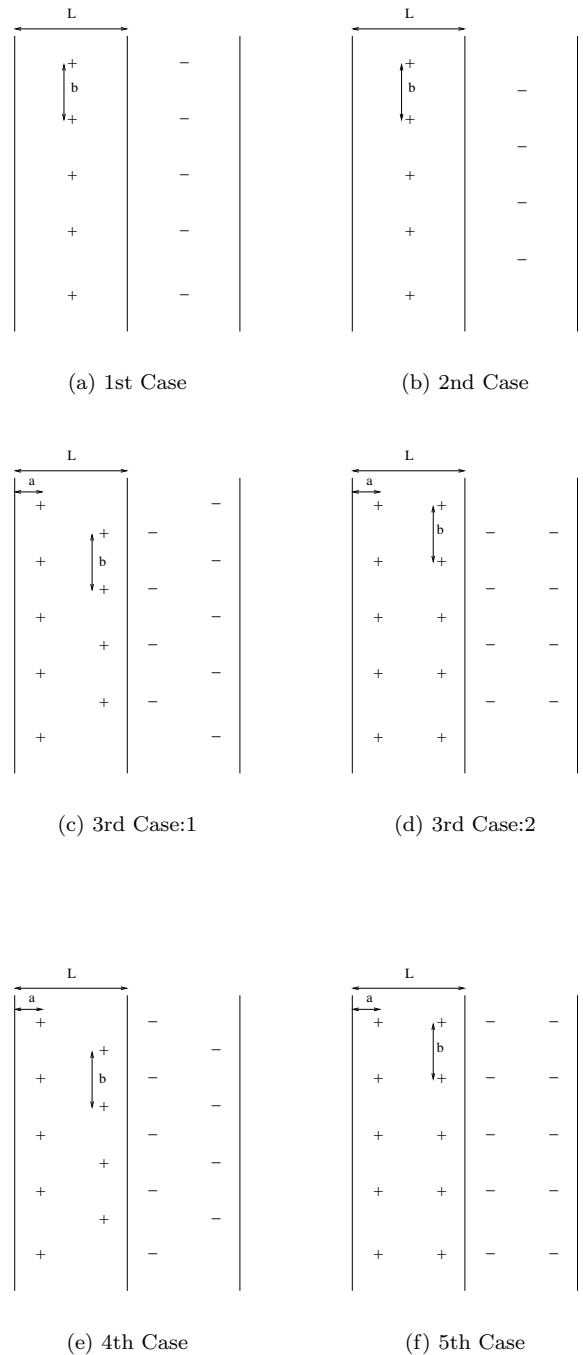


FIG. 1. Proposed configurations for  $N = 1$  and  $N = 2$  states.

In the other three candidate lattice structures, there are two chains per stripe domain  $N = 2$  states, at the distance  $a$  from the magnetic domain walls. The possible situations in the two chain cases are as follows; First, chains in the same domains are shifted by a half period  $b/2$  along  $y$  direction (see Fig. 1(c)). However, the neigh-

bor vortices and antivortices are next to each other. Second, they are just shifted by a half period  $b/2$  (see Fig. 1(e)). Third, the vortices and the antivortices are simply side by side on the chains (see Fig. 1(f)).

Our next step is to write the energies of these five candidates. To this end, we use the energy equations for periodic systems developed elsewhere [8].

$$u_{vv} = \frac{\phi_0^2}{4\pi\mathcal{A}^2} \sum_{\mathbf{G}} \frac{|F_{\mathbf{G}}|^2}{G(1+2\lambda G)}, \quad (3)$$

$$u_{mv} = -\frac{\phi_0}{\mathcal{A}} \sum_{\mathbf{G}} \frac{m_z \mathbf{G} F_{-\mathbf{G}}}{1+2\lambda G}, \quad (4)$$

$$u_{mm} = -2\pi\lambda \sum_{\mathbf{G}} \frac{G^2 |\mathbf{m}_z \mathbf{G}|^2}{1+2\lambda G}. \quad (5)$$

In those equations, the vortex configurations differ by their form-factors. We can obtain them from  $F_{\mathbf{G}} = \sum_{\mathbf{r}_i} n_i e^{i\mathbf{G} \cdot \mathbf{r}_i}$ , where the  $\mathbf{G}$ 's are the reciprocal vectors of the periodic structures, the  $\mathbf{r}_i$  are the positions of the vortex centers, and  $n_i$  are the charge of the vortex. In our proposed models,  $\mathbf{G} = ((2r+1)\frac{\pi}{L}, 2s\frac{\pi}{L})$  and  $n_i = \pm 1$ . Table I gives the form factors of each configuration in the order they are described above.

TABLE I. The form-factors of vortices in the proposed configurations.

configuration	$F_{\mathbf{G}}$
1	$i(-1)^r$
2	$i(-1)^r(1+(-1)^s)$
3	$2i \sin G_x a (1+(-1)^s)$
4	$e^{iG_x a} - (-1)^s e^{-iG_x a}$
5	$2i \sin G_x a$

Note that, in Table I, the form-factor for the third configuration also belongs to the case in which the vortex and the antivortex chains are shifted by half period only in the neighbour domains, not in the same domain (see Fig. 1(d)). Since information about the vortex lattice is carried only by the form factors, there is no need to consider the above-mentioned case separately.

In our calculations, the divergent part of the series must be extracted carefully. We show below the detailed analysis of series equations for each candidate. We start with the self interaction energy of the magnetic layer  $U_{mm}$ , since it is the same for each configuration. For the periodic structures, it is given by (5). Direct substitution of the Fourier coefficient of the stripe phase  $m_z \mathbf{G} = \frac{2im}{\pi(2r+1)}$  into Eq.(5) gives the self-interaction of the magnetic layer per unit cell as

$$u_{mm} = -\frac{8m^2}{L} \sum_{r=0}^{\infty} \frac{1}{\frac{L}{2\pi\Lambda} + 2r + 1}. \quad (6)$$

where  $\psi^{(0)}(x)$  is the polygamma function of zeroth order [9]. In our numerical calculations, we write the logarithmic term in (6) as  $\ln(\Lambda/l) + \ln(L/\Lambda)$  and then incorporate the  $-4m^2 \ln(\Lambda/l)$  term in the renormalized  $\varepsilon_{dw}^{ren}$ . Another energy term with a divergent series is the vortex energy, in general given by (3). The logarithmic divergence in this term stems from the vortex self-energies. We first split (3) into two parts as follows:

$$u_{vv} = \frac{\pi\varepsilon_0}{2L^2b^2} \sum_{\mathbf{G}} \left[ \frac{|F_{\mathbf{G}}|^2}{G^2} - \frac{|F_{\mathbf{G}}|^2}{G^2(1+2\lambda G)} \right]. \quad (7)$$

Note that the area of the unit cell is  $2Lb$ . The first term of the series above contributes to the self-energies of the vortices; whereas, the second term is the vortex-vortex energy and will be left in the series form. For each form-factor in Table I the series in the first term can be transformed to the form of  $\sum_{r=-\infty}^{\infty} \sum_{s=-\infty}^{\infty} 1/((2r+1)^2x^2 + s^2)$  where  $x$  is constant, and depends on the form-factor. A detailed analysis of such series is given in Appendix A.

The next step is to find the vortex energy and the interaction energy of the magnetization and vortices for each configuration. In the calculation of  $u_{mv}$ , we take the Fourier coefficient of the magnetization to be  $\frac{4im}{(2r+1)}\delta(G_y)$ . The fact that the stripe is infinite along the  $y$  direction results in the additional term  $2\pi\delta(G_y)$ . However, it does not play any role in the calculation of  $u_{mm}$ . For numerical analysis, these energies must be expressed in terms of dimensionless parameters. To this end, we define dimensionless variables  $\tilde{\Lambda} = \Lambda/L$ ,  $\tilde{b} = b/L$  and  $\tilde{\varepsilon}_{dw} = \varepsilon_{dw}^{ren} \Lambda/\varepsilon_0$ . The total energy  $\tilde{U}$  is measured in units of  $\varepsilon_0/\Lambda^2$ . In addition, we introduce the dimensionless magnetic energy as  $\tilde{U}_{mm} = u_{mm}/(\varepsilon_0/\Lambda^2)$ . In terms of these parameters, the energy of the first configuration reads

$$\tilde{U}^{(1)} = \frac{\tilde{\Lambda}^2}{4\tilde{b}} \left( \ln \left( \frac{4\Lambda}{e^C \tilde{\Lambda} \xi} \right) + 2f_v^{(1)}(\tilde{\Lambda}) - \frac{2f_{vv}^{(1)}(\tilde{\Lambda}, \tilde{b})}{\tilde{b}\pi} - \frac{16m\phi_0}{\varepsilon_0} f_{mv}^{(1)}(\tilde{\Lambda}) \right) + \tilde{U}_{mm} + \tilde{\varepsilon}_{dw} \tilde{\Lambda}, \quad (8)$$

where,

$$\begin{aligned} f_v^{(1)} &= \sum_{r=0}^{\infty} \frac{\coth((2r+1)\frac{\tilde{b}\pi}{2}) - 1}{2r+1}, \\ f_{vv}^{(1)} &= \sum_{r,s=-\infty}^{\infty} \frac{1}{\left( (2r+1)^2 + \frac{4s^2}{b^2} \right) (1 + 2\pi\tilde{\Lambda}\sqrt{(2r+1)^2 + \frac{4s^2}{b^2}})}, \\ f_{mv}^{(1)} &= \sum_{r=0}^{\infty} \frac{(-1)^r}{(2r+1)(1 + 2\pi\tilde{\Lambda}(2r+1))}. \end{aligned} \quad (9)$$

The form factor for the second configuration survives of the second configuration is found to be only for even values of  $s$ . Then, the dimensionless energy

$$\tilde{U}^{(2)} = \frac{\tilde{\Lambda}^2}{2\tilde{b}} \left( \ln \left( \frac{4\Lambda}{e^C \tilde{\Lambda} \xi} \right) + 2f_v^{(2)}(\tilde{\Lambda}) - \frac{4f_{vv}^{(2)}(\tilde{\Lambda}, \tilde{b})}{\tilde{b}\pi} - \frac{16m\phi_0}{\varepsilon_0} f_{mv}^{(2)}(\tilde{\Lambda}) \right) + \tilde{U}_{mm} + \tilde{\varepsilon}_{dw} \tilde{\Lambda}, \quad (10)$$

where  $f_{mv}^{(2)} = f_{mv}^{(1)}$  and,

$$\begin{aligned} f_v^{(2)} &= \sum_{r=0}^{\infty} \frac{\coth((2r+1)\frac{\tilde{b}\pi}{4}) - 1}{2r+1}, \\ f_{vv}^{(2)} &= \sum_{r,s=-\infty}^{\infty} \frac{1}{\left( (2r+1)^2 + \frac{16s^2}{b^2} \right) (1 + 2\pi\tilde{\Lambda}\sqrt{(2r+1)^2 + \frac{16s^2}{b^2}})}. \end{aligned} \quad (11)$$

In the third configuration, as in the second configuration, only even values of  $s$  contribute to the energy. In the first two configurations, the square of their form-factors enter the vortex energy as a constant. However, in this case, the square of the sine function appears. In

Appendix A, it is shown how to calculate the series in the presence of such functions. Introducing the dimensionless parameter  $\tilde{a} = a/L$ , the energy functional of the third configuration becomes

$$\begin{aligned} \tilde{U}^{(3)} &= \frac{\tilde{\Lambda}^2}{\tilde{b}} \left( \ln \left( \frac{4\Lambda}{e^C \tilde{\Lambda} \xi} \right) - \ln(\cot(\pi\tilde{a})) + 4f_v^{(3)}(\tilde{\Lambda}, \tilde{a}) - \frac{8}{\tilde{b}\pi} f_{vv}^{(3)}(\tilde{\Lambda}, \tilde{a}, \tilde{b}) - \frac{16m\phi_0}{\varepsilon_0} f_{mv}^{(3)}(\tilde{\Lambda}, \tilde{a}) \right) \\ &+ \tilde{U}_{mm} + \tilde{\varepsilon}_{dw} \tilde{\Lambda}, \end{aligned} \quad (12)$$

where,

$$\begin{aligned} f_v^{(3)} &= \sum_{r=0}^{\infty} \frac{\coth((2r+1)\frac{\tilde{b}\pi}{4}) - 1}{2r+1} \sin^2((2r+1)\pi\tilde{a}), \\ f_{vv}^{(3)} &= \sum_{r,s=-\infty}^{\infty} \frac{\sin^2((2r+1)\pi\tilde{a})}{\left( (2r+1)^2 + \frac{16s^2}{b^2} \right) (1 + 2\pi\tilde{\Lambda}\sqrt{(2r+1)^2 + \frac{16s^2}{b^2}})}, \\ f_{mv}^{(3)} &= \sum_{r=0}^{\infty} \frac{\sin((2r+1)\pi\tilde{a})}{(2r+1)(1 + 2\pi\tilde{\Lambda}(2r+1))}. \end{aligned} \quad (13)$$

In the fourth configuration, the square of the form-factor is:  
 $|F_G|^2 = 2 - 2(-1)^s \cos((2r+1)\pi\tilde{a})$ . Even and odd values

of  $s$  give different contributions. Then, we can calculate the vortex energy for even  $s$  and odd  $s$  separately. Employing similar techniques, we find

$$\tilde{U}^{(4)} = \frac{\tilde{\Lambda}^2}{2\tilde{b}} \left( \ln \left( \frac{4\Lambda}{e^C \tilde{\Lambda} \xi} \right) + 2f_v^{(4)}(\tilde{\Lambda}, \tilde{a}) - \frac{4}{\tilde{b}\pi} f_{vv}^{(4)}(\tilde{\Lambda}, \tilde{a}, \tilde{b}) - \frac{16m\phi_0}{\varepsilon_0} f_{mv}^{(4)}(\tilde{\Lambda}, \tilde{a}) \right) + \tilde{U}_{mm} + \tilde{\varepsilon}_{dw} \tilde{\Lambda}, \quad (14)$$

where  $f_{mv}^{(4)} = f_{mv}^{(3)}$  and,

$$\begin{aligned} f_v^{(4)} &= \sum_{r=0}^{\infty} \frac{\coth((2r+1)\frac{\pi\tilde{b}}{4}) - 1}{2r+1} \sin^2((2r+1)\pi\tilde{a}) + \sum_{r=0}^{\infty} \frac{\tanh((2r+1)\frac{\pi\tilde{b}}{4}) - 1}{2r+1} \cos^2((2r+1)\pi\tilde{a}), \\ f_{vv}^{(4)} &= \sum_{r,s=-\infty}^{\infty} \frac{\sin^2((2r+1)\pi\tilde{a})}{\left( (2r+1)^2 + \frac{16s^2}{\tilde{b}^2} \right) (1 + 2\pi\tilde{\Lambda}\sqrt{(2r+1)^2 + \frac{16s^2}{\tilde{b}^2}})} \\ &+ \sum_{r,s=-\infty}^{\infty} \frac{\cos^2((2r+1)\pi\tilde{a})}{\left( (2r+1)^2 + \frac{4(2s+1)^2}{\tilde{b}^2} \right) (1 + 2\pi\tilde{\Lambda}\sqrt{(2r+1)^2 + \frac{4(2s+1)^2}{\tilde{b}^2}})}. \end{aligned} \quad (15)$$

The form-factor for the fifth case resembles that of the third case with an exception. That is, in the third case, only even values of  $s$  are taken into account, while all

integers contributes to the sum over  $s$  in the fifth case. Keeping this in mind, it is straightforward to obtain the dimensionless energy for the last case as

$$\begin{aligned} \tilde{U}^{(5)} &= \frac{\tilde{\Lambda}^2}{2\tilde{b}} \left( \ln \left( \frac{4\Lambda}{e^C \tilde{\Lambda} \xi} \right) - \ln(\cot(\pi\tilde{a})) + 4f_v^{(5)}(\tilde{\Lambda}, \tilde{a}) - \frac{4}{\tilde{b}\pi} f_{vv}^{(5)}(\tilde{\Lambda}, \tilde{a}, \tilde{b}) - \frac{16m\phi_0}{\varepsilon_0} f_{mv}^{(5)}(\tilde{\Lambda}, \tilde{a}) \right) \\ &+ \tilde{U}_{mm} + \tilde{\varepsilon}_{dw} \tilde{\Lambda}, \end{aligned} \quad (16)$$

where  $f_{mv}^{(5)} = f_{mv}^{(3)}$  and,

$$\begin{aligned} f_v^{(5)} &= \sum_{r=0}^{\infty} \frac{\coth((2r+1)\frac{\pi\tilde{b}}{2}) - 1}{2r+1} \sin^2((2r+1)\pi\tilde{a}), \\ f_{vv}^{(5)} &= \sum_{r,s=-\infty}^{\infty} \frac{\sin^2((2r+1)\pi\tilde{a})}{\left( (2r+1)^2 + \frac{4s^2}{\tilde{b}^2} \right) (1 + 2\pi\tilde{\Lambda}\sqrt{(2r+1)^2 + \frac{4s^2}{\tilde{b}^2}})}. \end{aligned} \quad (17)$$

### III. RESULTS FOR $N = 1$ AND $N = 2$ STATES

In this section, we present our results based on numerical calculations. The series in  $f_v^{(i)}$  converges very fast when  $r_{max} > 200$ , while the series in  $f_{vv}^{(i)}$  and converges rather slowly, although, when  $r_{max} > 4000$  and  $s_{max} > 4000$ , the results do not change up to 6th decimal point in the energy, where  $i$  labels the particular domain configuration. To make sure of this accuracy in the calculations, we take  $r_{max} = 600$  for  $f_v^{(i)}$ ,  $r_{max} = 5000$  for  $f_{mv}^{(i)}$ , and  $r_{max} = 5000$  and  $s_{max} = 5000$  for  $f_{vv}^{(i)}$  in Eqs.(8, 10, 12, 14, 16). In addition, the respective error deviations for  $\lambda/L, b/L$  and  $a/L$  in numerical calculations are  $\pm 0.005, \pm 0.0005$  and  $\pm 0.0125$ .

In the numerical minimization of Eqs.(8, 10, 12, 14, 16), we take  $\ln(4\Lambda/(e^C \xi)) = 5.57$ . Changing  $m\phi_0/\varepsilon_0$  at fixed  $\tilde{\varepsilon}_{dw}$ , we calculate the minimal energy of each

configuration. We first investigate when these configurations become energetically favorable in the system. To this end, we check where the equilibrium energies of the configurations first become negative.

In our analysis, we first identify two regimes of interest: discrete regime ( $\varepsilon_{dw} \leq 4\tilde{m}^2$ ) and continuum regime ( $\varepsilon_{dw} > 4\tilde{m}^2$ ). Using our parameters  $\tilde{\varepsilon}_{dw}$  and  $m\phi_0/\varepsilon_0$ , the inequality for discrete regime can be expressed as

$$\tilde{\varepsilon}_{dw} \leq \frac{\ln(\frac{\Lambda}{\xi})^2}{4\pi^2} \left( \frac{m\phi_0}{\varepsilon_0 \ln(\frac{\Lambda}{\xi})} - 1 \right)^2. \quad (18)$$

From Eq.18, the minimum value of  $m\phi_0/\varepsilon_0$  for different values of  $\tilde{\varepsilon}_{dw}$  can be determined. These values are given in Table.II

TABLE II.  $\tilde{\varepsilon}_{dw}$  versus  $(m\phi_0/\varepsilon_0)_{min}$ . The column on the left is input.

$\tilde{\varepsilon}_{dw}$	$(m\phi_0/\varepsilon_0)_{min}$
0.01	6.198
0.10	7.557
1.00	11.853
10.00	25.439

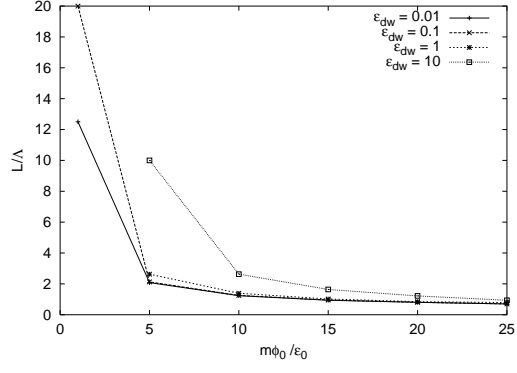
When  $m\phi_0/\varepsilon_0$  is greater than its minimum value for a certain  $\tilde{\varepsilon}_{dw}$ , the system is then in the discrete regime. Next, we analyze the proposed cases for  $N = 1$  and  $N = 2$  states according to numerical values given in Table.II. The equilibrium of energies for these cases in discrete and continuum regimes are given in Table.III.

TABLE III. Equilibrium energies for proposed configurations. Two columns on the left are input.

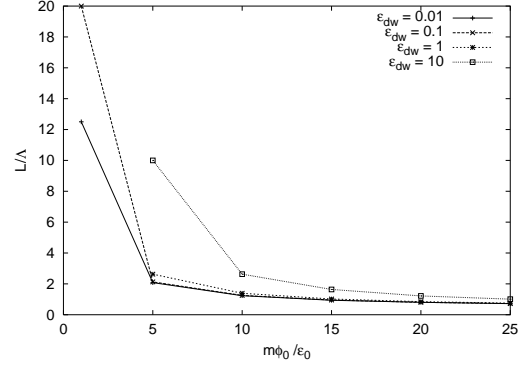
$\varepsilon_{dw}$	$(m\phi_0/\varepsilon_v)_{min}$	$\tilde{U}_1$	$\tilde{U}_2$	$\tilde{U}_3$	$\tilde{U}_4$	$\tilde{U}_5$
0.01	5	-2.58454176	-2.58455668	-3.36407195	-3.36404625	-3.36404615
0.01	20	-65.98296440	-65.98296500	-89.20105311	-89.20030961	-89.20030943
0.1	5	-2.54211623	-2.54211637	-3.33057991	-3.33054828	-3.32949063
0.1	20	-65.87136440	-65.87136500	-89.10475311	-89.10310961	-89.10310943
1	5	-2.16635495	-2.16637343	-3.01972350	-3.01972355	-3.01972347
1	20	-64.78187766	-64.781878054	-88.15826391	-88.15826394	-88.15826367
10	5	-0.35644861	-0.35667498	-1.21258278	-1.21232397	-1.21232396
10	25	-95.00241100	-95.00247780	-134.28090345	-134.27589780	-134.27589769

In our numerical calculations, we find that all proposed configurations are stable both in discrete and continuum regimes. This indicates that our method works well in both regimes. Our numerical calculations also show that the third configuration wins over the other cases. Nonetheless, this is not enough information for us to understand the equilibrium structure, since  $\tilde{U}^{(3)}$  corresponds to two different cases with the same structure factor. At this point, we need further analysis to determine which configuration is more likely. This can be done from simple physical considerations. Namely, in FSB, the equilibrium structure is determined by the competition between vortex-vortex interaction and vortex - magnetization interaction. The former favors vortices and antivortices in neighbor domains to line up in transverse direction ( perpendicular to magnetic domain wall ), whereas the latter prefers vortices and antivortices to be shifted so that gain in energy is maximized. When vortices are next to each other on the either side of the magnetic domain wall, the magnetic fields they produce cancel out each other. From the numerical results, it is obvious that vortex-magnetization interaction wins the competition, and results in half-way shifting of vortices, if one compares the energies of 1st and 2nd cases.

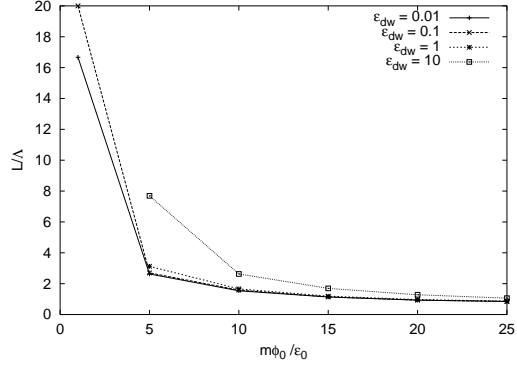
Then, vortex-magnetization interaction is the dominant factor. By the same token, one can understand what is going on in double vortex chain configurations. For instance, in the fifth configuration, energy gain due to vortex-magnetization interaction is diminished, since all the vortices are side by side. This explains why equilibrium energy of the fifth configuration is higher than those of third and fourth cases. In the fourth configuration, the vortices and antivortices in the neighbor domains are half-way shifted, so that this configuration must be preferred over the one in which they sit side by side in the neighbor domains according to the above arguments. However, alternative configuration for third case has two chains half-way shifted in the neighbor domains instead of one chain as in the fourth case. Therefore, one might expect gain is even more than that in the fourth configuration. Another interesting result is that the system does not favor  $N = 1$  state at all. Actually, this does not surprise us since, in the continuum approximation, we found that the vortex density increases near the magnetic domain walls. This fact already suggests that the system favors vortex chains being near the magnetic domain walls rather than a single chain in the middle of the domain.



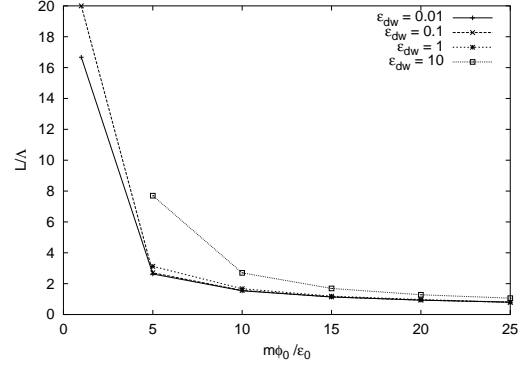
(a) 1st Case:  $L/\Lambda$



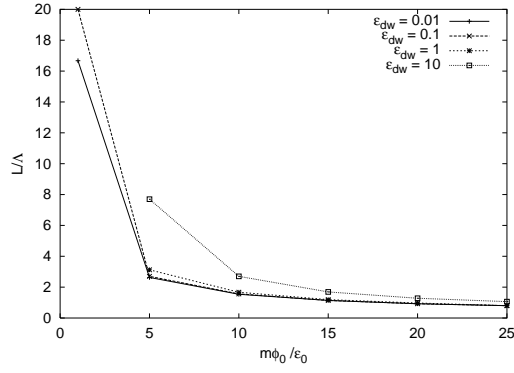
(b) 2nd Case:  $L/\Lambda$



(c) 3rd Case:  $L/\Lambda$

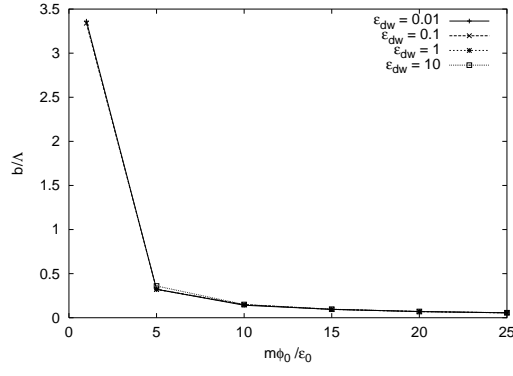


(d) 4th Case:  $L/\Lambda$

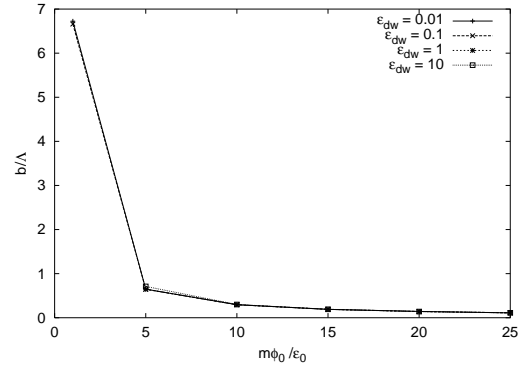


(e) 5th Case:  $L/\Lambda$

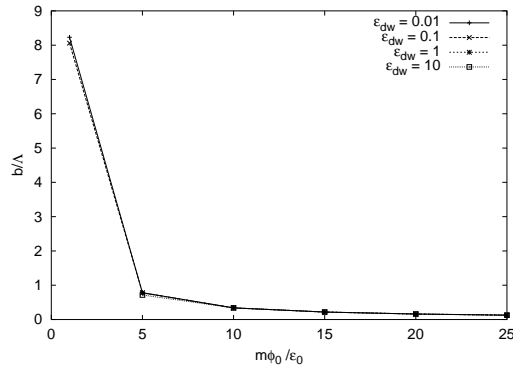
FIG. 2.  $L/\Lambda$  versus  $m\phi_0/\varepsilon_0$  for  $N = 1$  and  $N = 2$  states.



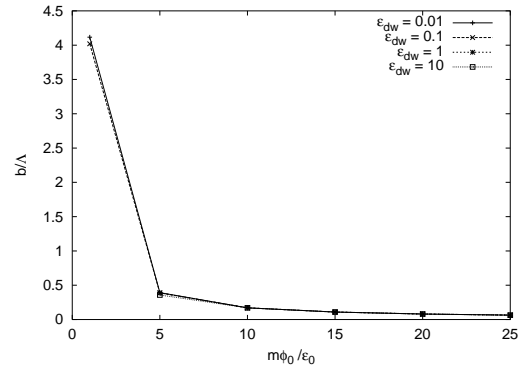
(a) 1st Case:  $b/\Lambda$



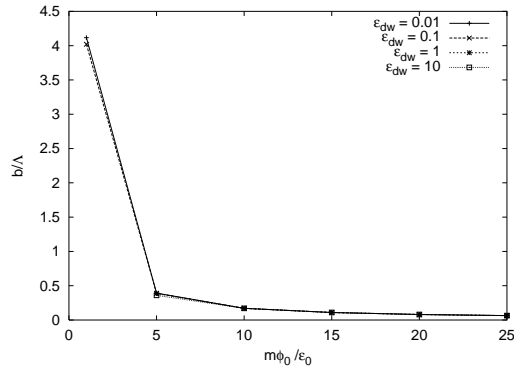
(b) 2nd Case:  $b/\Lambda$



(c) 3rd Case:  $b/\Lambda$



(d) 4th Case:  $b/\Lambda$



(e) 5th Case:  $b/\Lambda$

FIG. 3.  $b/\Lambda$  versus  $m\phi_0/\varepsilon_0$  for  $N = 1$  and  $N = 2$  states.

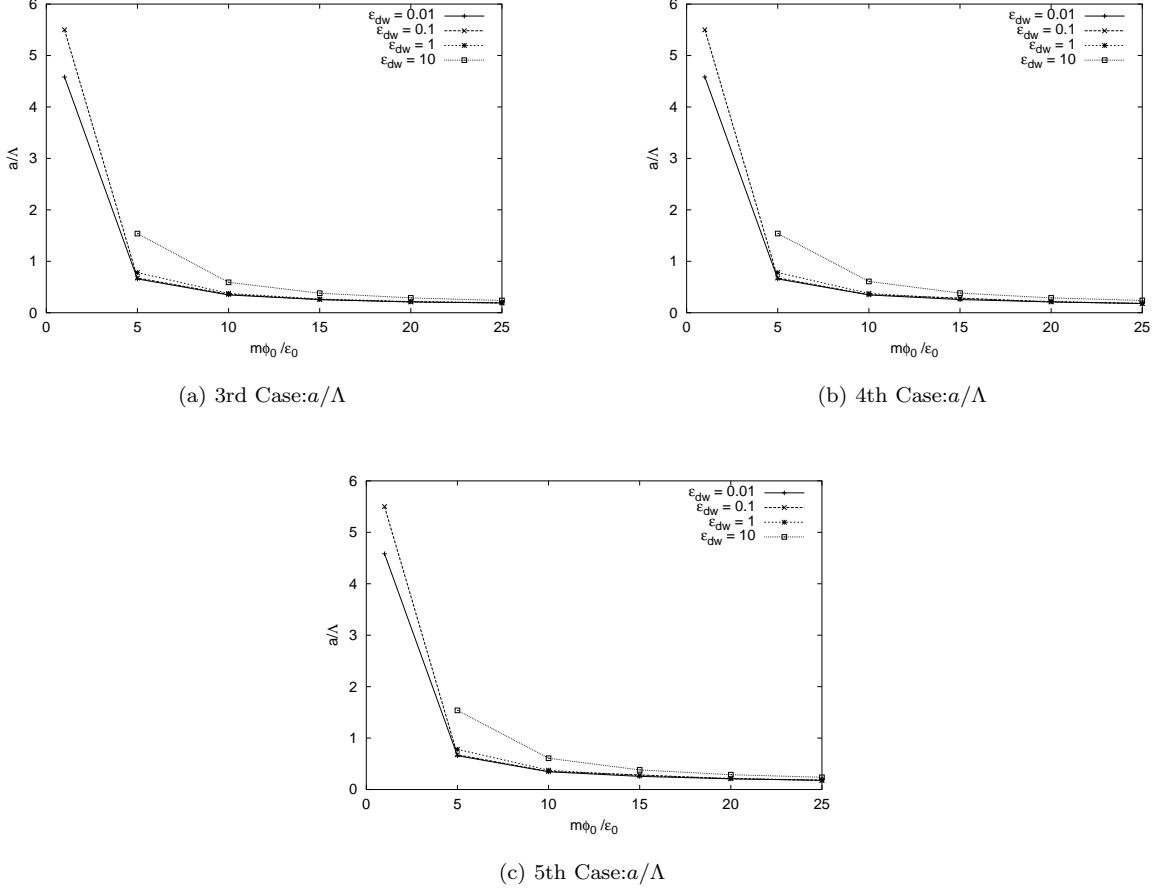


FIG. 4.  $a/\Lambda$  versus  $m\phi_0/\varepsilon_0$  for  $N = 1$  and  $N = 2$  states.

In numerical calculations equilibrium domain size  $L/\Lambda$ , vortex-vortex distances on the same chain  $b/\Lambda$  and vortex-magnetic domain wall distances  $a/\Lambda$  are also calculated. These results are depicted in Figs.2,3,4. At fixed  $\tilde{\varepsilon}_{dw}$ , the further increase of  $m\phi_0/\varepsilon_0$  shrinks the domain width, while higher domain wall energy favors larger domain width at fixed  $m\phi_0/\varepsilon_0$ , as in usual ferromagnets. That is to say, ferromagnet favors narrower domains to minimize the demagnetization energy whereas domain wall energy makes domains wider. The competition between these two energies determine the domain size. Here, the parameter  $m\phi_0/\varepsilon_0$  plays the role of demagnetization energy. Domain wall energy does not affect the distance between the vortices located on the same chain. However, at larger values of  $m\phi_0/\varepsilon_0$  the vortices on the same chain gets closer. This implies that the unit cell area shrinks, and consequently vortex density per area increases. Results of unit cell areas and vortex densities are discussed with details in the next section.

#### IV. $N = 3$ STATE

In this section, our aim is to understand whether the domain structures with different number vortex chains appear spontaneously or not. To answer this question, we consider only  $N = 3$  state and compare its equilibrium energy with that of  $N = 2$  state for various values of magnetic domain wall energy and magnetization. We first show the derivation of energy equation for  $N = 3$  state. Following the physical arguments in the previous section, we consider that the equilibrium configuration is superposition of the 2nd case and alternative 3rd case (see Fig.5).

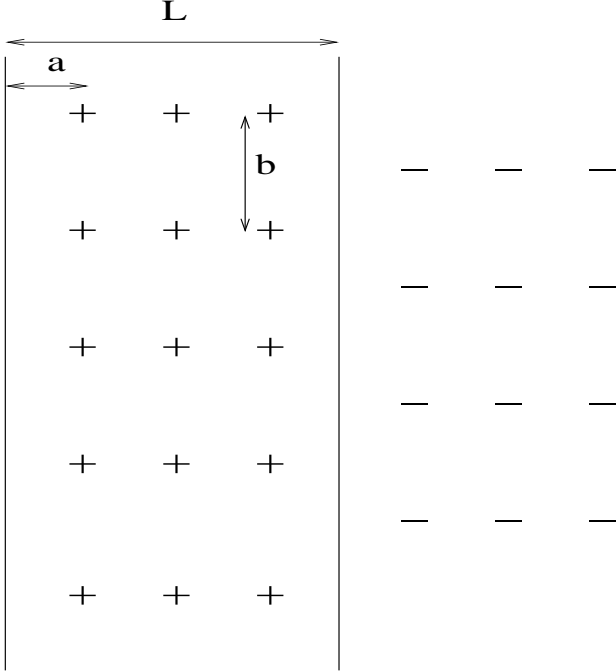


FIG. 5. The vortex lattice in the first configuration.

Then, its structure factor equals to sum of structure factors of those cases, which is given by

$$F_{\mathbf{G}} = (2i \sin(G_x a) + i(-1)^r)(1 + (-1)^s). \quad (19)$$

As seen in second section, self-vortex energy and vortex-vortex interaction depend on  $|F_{\mathbf{G}}|^2$ , whereas  $F_{\mathbf{G}}$  is used in vortex-magnetization interaction energy. Then, it is easy to see vortex-magnetization energy in this case as the sum of those of 2nd and 3rd case. We then calculate only the vortex energy here. The square of structure factor is  $|F_{\mathbf{G}}|^2 = |F_{\mathbf{G}}^{(2)}|^2 + |F_{\mathbf{G}}^{(3)}|^2 + (F_{\mathbf{G}}^{(2)})^*(F_{\mathbf{G}}^{(3)}) + (F_{\mathbf{G}}^{(3)})^*(F_{\mathbf{G}}^{(2)})$ . The first two terms give the vortex energy contributions of 2nd and 3rd case. Then, it is necessary to calculate contribution from the cross term only, which reads

$$\begin{aligned} \tilde{U}_{cross} = & \frac{4\tilde{\Lambda}^2}{\tilde{b}} \sum_{r=0}^{\infty} \sin((2r+1)\pi\tilde{a})(-1)^r \left( \frac{\cot((2r+1)\pi\tilde{b}/4) - 1}{2r+1} \right) + \frac{2\tilde{\Lambda}^2}{\tilde{b}} \ln |\cot(\pi/4 - \pi\tilde{a}/2)| \\ & - \frac{2\tilde{\Lambda}^2}{\pi^2\tilde{b}^2} \sum_{r,s=-\infty}^{\infty} \frac{\sin((2r+1)\pi\tilde{a})(-1)^r}{(2r+1)^2 + 16s^2/\tilde{b}^2} \frac{1}{1 + 2\pi\tilde{\Lambda}\sqrt{(2r+1)^2 + 16s^2/\tilde{b}^2}}. \end{aligned} \quad (20)$$

Then, total energy becomes

$$\begin{aligned} \tilde{U}^{N=3} = & \frac{\tilde{\Lambda}^2}{2\tilde{b}} \left( \ln \left( \frac{4\Lambda}{e^C \tilde{\Lambda} \xi} \right) + 2f_v^{(2)}(\tilde{\Lambda}) - \frac{4f_{vv}^{(2)}(\tilde{\Lambda}, \tilde{b})}{\tilde{b}\pi} - \frac{16m\phi_0}{\varepsilon_0} f_{mv}^{(2)}(\tilde{\Lambda}) \right) \\ & + \frac{\tilde{\Lambda}^2}{\tilde{b}} \left( \ln \left( \frac{4\Lambda}{e^C \tilde{\Lambda} \xi} \right) - \ln(\cot(\pi\tilde{a})) + 4f_v^{(3)}(\tilde{\Lambda}, \tilde{a}) - \frac{8}{\tilde{b}\pi} f_{vv}^{(3)}(\tilde{\Lambda}, \tilde{a}, \tilde{b}) - \frac{16m\phi_0}{\varepsilon_0} f_{mv}^{(3)}(\tilde{\Lambda}, \tilde{a}) \right) + \tilde{U}_{cross} + \tilde{U}_{mm} + \tilde{\varepsilon}_{dw}\tilde{\Lambda}. \end{aligned} \quad (21)$$

Note that  $\tilde{U}_{mm}$  is described in section II. Next, Eq.22 is minimized w.r.t.  $\tilde{\Lambda}, \tilde{b}$  and  $\tilde{a}$  for different values of  $\tilde{\varepsilon}_{dw}$  and  $m\phi_0/\varepsilon_0$ . In numerical calculations, the series are calculated as described in the previous section. The comparison of equilibrium energies of  $N = 1$ ,  $N = 2$  and

$N = 3$  states at fixed values of  $\tilde{\varepsilon}_{dw}$  and  $m\phi_0/\varepsilon_0$  are given in Table.IV. Note that  $N = 1$  state represents the second configuration in section II, since it is the most energetically favorable configuration between two single vortex chain configurations.

TABLE IV. Equilibrium energies of two chain and three chain states. Vortex density of unit cell  $n$  equals  $N_{cell}/S_{el}$ , where  $N_{cell} = 2N$  is the number of vortices in a unit cell and  $S_{el} = 2\tilde{L}\tilde{b}$  is equilibrium unit cell area. The two columns on the left are input.

$\tilde{\epsilon}_{dw}$	$m\phi_0/\epsilon_0$	$U^{N=1}$	$S_{el}$	$n$	$U^{N=2}$	$S_{el}$	$n$	$U^{N=3}$	$S_{el}$	$n$
0.01	5	-2.5846	2.70	0.74	-3.3641	4.11	0.97	-3.2576	6.64	0.90
0.01	10	-13.9742	0.73	2.74	-18.5183	1.04	3.82	-18.8330	1.58	3.79
0.01	15	-35.0799	0.36	5.56	-47.0362	0.50	8.02	-48.7311	0.75	8.02
0.01	20	-65.9830	0.22	8.98	-89.2011	0.30	13.24	-93.4879	0.44	13.49
0.1	5	-2.5421	2.75	0.73	-3.3306	4.22	0.95	-3.2324	6.64	0.90
0.1	10	-13.9015	0.74	2.71	-18.4598	1.08	3.71	-18.7780	1.58	3.79
0.1	15	-34.9848	0.36	5.52	-46.9570	0.50	8.02	-48.6699	0.75	8.02
0.1	20	-65.8714	0.23	8.74	-89.1048	0.30	13.24	-93.4122	0.44	13.49
1	5	-2.1664	3.39	0.59	-3.0197	4.84	0.83	-2.9941	7.13	0.84
1	10	-13.2169	0.82	2.44	-17.8987	1.13	3.54	-18.3421	1.68	3.56
1	15	-34.0699	0.39	5.14	-46.1860	0.52	7.67	-48.0673	0.77	7.78
1	20	-67.7819	0.24	8.40	-88.1583	0.31	12.79	-92.6655	0.45	13.18
10	5	-0.3567	14.2	0.14	-1.2126	10.99	0.36	-1.4638	14.16	0.42
10	10	-8.6308	1.58	1.27	-13.6758	1.78	2.24	-14.8269	2.37	2.53
10	15	-27.1877	0.63	3.18	-39.9099	0.74	5.41	-42.8834	0.99	6.05
10	20	-56.0242	0.34	5.80	-80.1062	0.41	9.66	-86.0271	0.56	10.78

As seen from Table.IV, at low magnetization and small domain wall energies,  $N = 2$  state is energetically favorable. However,  $N = 3$  state wins over at high values of  $m\phi_0/\epsilon_0$  and  $\tilde{\epsilon}_{dw}$ . This picture resembles the one we see in the case of magnetic dots on a SC film. In that case, the further increase in  $m\phi_0/\epsilon_0$  and the dot's size makes other vortex states more energetically favorable [10]. Here, the domain's size is also controlled by domain wall energy. Therefore, the larger the  $\tilde{\epsilon}_{dw}$ , the larger the domain size. As a result, new chain states might be more energetically favorable. In  $N = 3$  state, how the equilibrium domain size, vortex-vortex distance on the chain, and vortex chain-domain wall distance change according to different values of  $m\phi_0/\epsilon_0$  and  $\tilde{\epsilon}_{dw}$  are shown in Figs.6,7,8. As seen in these figures  $L/\Lambda, b/\Lambda$  and  $a/\Lambda$  follow the same pattern as that of  $N = 1$  and  $N = 2$  states. As number of chains per domain increases,  $L/\Lambda, b/\Lambda$  and  $a/\Lambda$  increase.

In addition to equilibrium energies, equilibrium unit cell areas and vortex densities of unit cells for  $N = 1$ ,  $N = 2$  and  $N = 3$  states are given in Table.IV. At fixed  $m\phi_0/\epsilon_0$ , unit cell area expands with further increase of  $\tilde{\epsilon}_{dw}$ . However, it shrinks when  $m\phi_0/\epsilon_0$  increases. On the other hand, unit cell area expands with more more vortex chains at fixed values of  $m\phi_0/\epsilon_0$  and  $\tilde{\epsilon}_{dw}$  except, unit cell areal of  $N = 1$  state is larger than those of  $N = 2$  and  $N = 3$  states, when  $m\phi_0/\epsilon_0 = 5$  and  $\tilde{\epsilon}_{dw} = 10$ . We think that  $N = 1$  state in this case is energetically very close to instable region in which there is monodomain only. Furthermore, from our results, we expect that the most energetically favorable state has the highest vortex density.

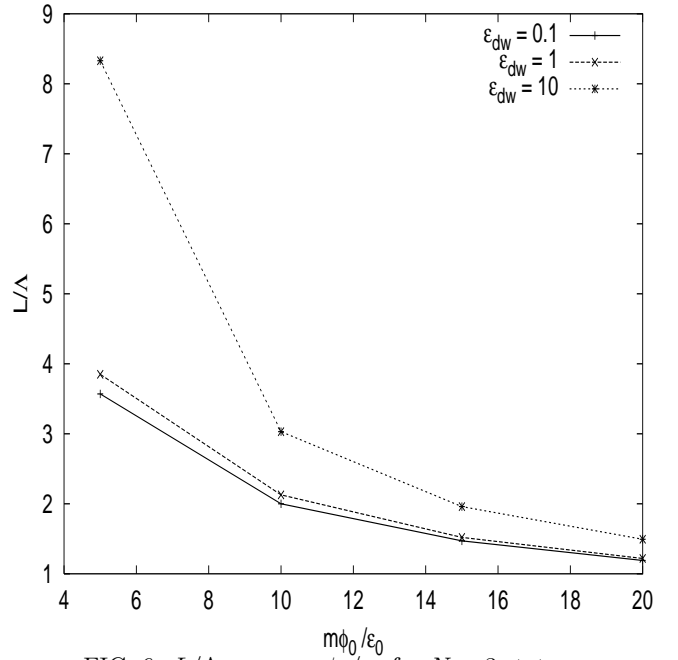


FIG. 6.  $L/\Lambda$  versus  $m\phi_0/\epsilon_0$  for  $N = 3$  state.

FIG. 8.  $a/\Lambda$  versus  $m\phi_0/\varepsilon_0$  for  $N = 3$  state.

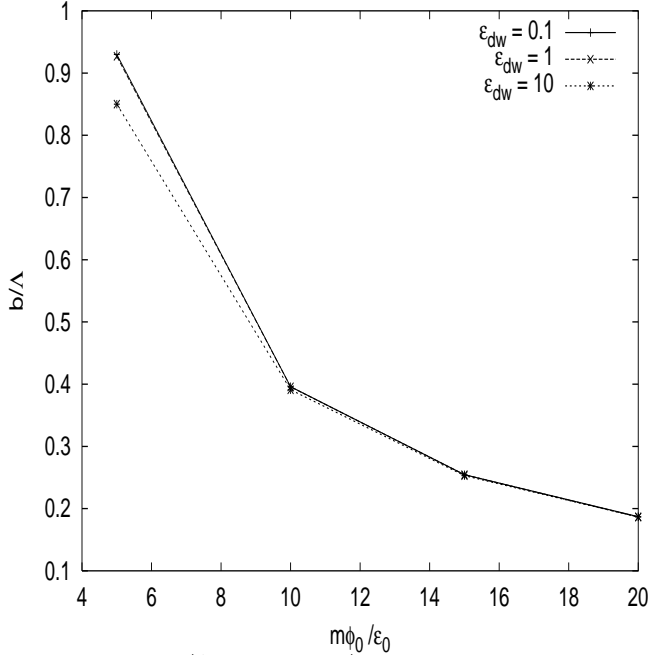
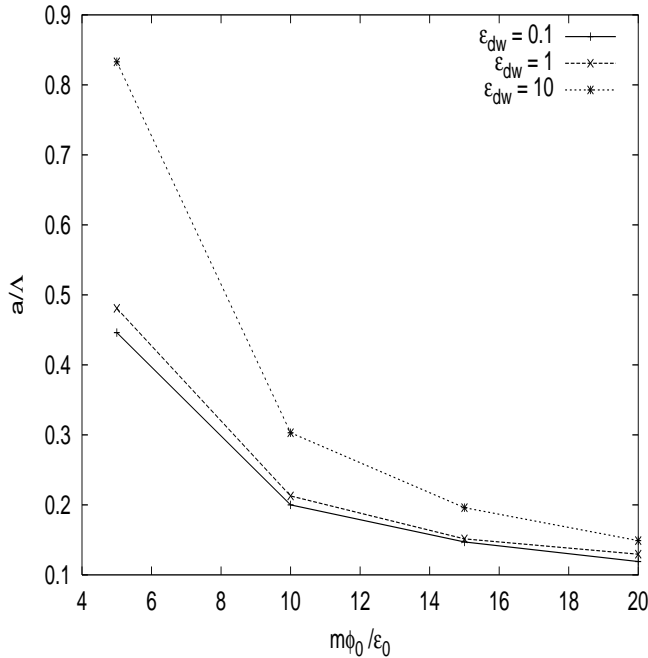


FIG. 7.  $b/\Lambda$  versus  $m\phi_0/\varepsilon_0$  for  $N = 3$  state.



## V. CONCLUSIONS

In this article, we reported our results on the lattices of discrete vortices in stripe domains in FSB based on a method based on Maxwell-London equations. If  $\varepsilon_{dw} \leq 4\tilde{m}^2$ , the continuum approximation becomes invalid. Instead, we considered the discrete lattice of vortices in which the vortices were considered to be situated on chains directed along the stripes. We first analyzed the vortex configurations up to two vortex chains. Depending on the magnetization and the magnetic domain wall energy, the equilibrium energy, the positions of the vortices and the equilibrium domain size are calculated. According to our calculations, in equilibrium, vortices on the either side of the magnetic domain walls are not side by side on the chains; instead, they are shifted by a half period along the stripe, while they are side by side in the same domain. We also checked whether different vortex chain states can be energetically favorable. To do so, we calculated the equilibrium energy for  $N = 3$  state whose equilibrium configuration was assumed to be the superposition of those for  $N = 1$  and  $N = 2$  states. The comparison of energies implies that more vortex chains can emerge spontaneously in the larger domains.

In numerical calculations, we also found that the vortex lattice is stable for  $\varepsilon_{dw} > 4\tilde{m}^2$ . At this point, the domain size is noticeably larger than the effective penetration depth  $\Lambda$ , so the continuum approximation is valid. Therefore, we expect that the domain nucleation starts in the continuum regime. This problem is left for the future research. At constant  $\tilde{\varepsilon}_{dw}$ , with increasing  $m\phi_0/\varepsilon_v$ , the equilibrium size of the domain decreases. In addition, the vortices on the chain get closer to each other. These results agree with those obtained in the continuum approximation. As  $\varepsilon_{dw}/4\tilde{m}^2$  increases, we expect that new vortex chains develop within the domains. We leave the detailed analysis of this problem to other publication.

## VI. ACKNOWLEDGMENTS

The most of this work was done during my stay at the University of Minnesota and was partially supported by the U.S. Department of Energy, Office of Science, under Contract No. W-31-109-ENG-38.

## APPENDIX: CALCULATIONS OF SERIES

In this appendix, the detailed analysis of series is given. First, the series in the energy calculations of the periodic systems are analyzed; second, the detailed calculation of the vortex density is shown. The series we encounter in the energy calculations fall into two categories. In the first category, we sum over one variable. The series in this category are in the form of  $\sum_{r=1}^{r_{max}} 1/r$ . Employing the Euler-Maclaurin summation formula [11], the summation is found with logarithmic accuracy as

$$\sum_{r=1}^{r_{max}} \frac{1}{r} \approx \ln r_{max} + C. \quad (A1)$$

where  $C \sim 0.577$  is the Euler-Mascheroni constant. If the summation is performed over only odd integers, we can still transform our series to (A1). Namely,

$$\sum_{r=0}^{r_{max}} \frac{1}{2r+1} \approx \sum_{r=1}^{2r_{max}+1} \frac{1}{r} - \frac{1}{2} \sum_{r=1}^{r_{max}/2} \frac{1}{r}, \quad (A2)$$

$$\approx \ln(2r_{max} + 1) + C - \ln\left(\frac{r_{max}}{2}\right) - \frac{C}{2}, \quad (A3)$$

$$\approx \frac{1}{2}(\ln r_{max} + C + 2 \ln 2). \quad (A4)$$

$$\sum_{r=-\infty}^{r=\infty} \sum_{s=-\infty}^{s=\infty} \frac{1}{x^2(2r+1)^2 + s^2} \approx \frac{2\pi}{x} \left[ \sum_{r=0}^{\infty} \frac{\coth((2r+1)\pi x) - 1}{2r+1} + \frac{\ln r_{max}}{2} + \frac{C}{2} \right], \quad (A7)$$

$$\sum_{r=-\infty}^{r=\infty} \sum_{s=-\infty}^{s=\infty} \frac{1}{x^2(2r+1)^2 + (2s+1)^2} \approx \frac{\pi}{x} \left[ \sum_{r=0}^{\infty} \frac{\tanh((2r+1)\frac{\pi x}{2}) - 1}{2r+1} + \frac{\ln r_{max}}{2} + \frac{C}{2} \right]. \quad (A8)$$

In (A7) and (A8), we use  $\sum_{s=0}^{\infty} 1/(y^2 + (2s+1)^2) = \pi \tanh(\pi y/2)/(4y)$ . In the presence of  $\sin^2((2r+1)y)$  or  $\cos^2((2r+1)y)$ , the series can be calculated in a similar

$$\begin{aligned} \sum_{r=-\infty}^{r=\infty} \sum_{s=-\infty}^{s=\infty} \frac{\sin^2((2r+1)y)}{(x^2(2r+1)^2 + s^2)} &= \frac{2\pi}{x} \left[ \sum_{r=0}^{\infty} \frac{\sin^2((2r+1)y)(\coth((2r+1)\pi x) - 1)}{2r+1} \right. \\ &\quad \left. + \frac{\ln r_{max}}{4} - \frac{\ln |\cot(y/2)|}{4} + \frac{C}{4} \right], \end{aligned} \quad (A9)$$

$$\begin{aligned} \sum_{r=-\infty}^{r=\infty} \sum_{s=-\infty}^{s=\infty} \frac{\cos^2((2r+1)y)}{(x^2(2r+1)^2 + s^2)} &= \frac{2\pi}{x} \left[ \sum_{r=0}^{\infty} \frac{\sin^2((2r+1)y)(\coth((2r+1)\pi x) - 1)}{2r+1} \right. \\ &\quad \left. + \frac{\ln r_{max}}{4} + \frac{\ln |\cot(y/2)|}{4} + \frac{C}{4} \right]. \end{aligned} \quad (A10)$$

We use

$$\sum_{r=0}^{\infty} \frac{\cos((2r+1)\theta)}{2r+1} = \frac{\ln |\cot(\theta/2)|}{2}. \quad (A11)$$

The other double series of interest here are in the form of

$$I(x) = \sum_{r=-\infty}^{r=\infty} \sum_{s=-\infty}^{s=\infty} \frac{1}{x^2 r^2 + s^2}, \quad (A5)$$

where  $x$  is an arbitrary constant. Although (A5) is logarithmically divergent, the sum over one of the variables can be done easily. To this end, we perform the sum over  $s$  first. In doing so, Eq. (A5) becomes  $(2\pi/x) \sum_{r=1}^{\infty} \coth(\pi x r)/r$  [12]. This series is logarithmically divergent. In order to get the logarithmic term, we add and subtract  $1/r$ . Using the result in (A1), finally we get

$$I(x) \approx \frac{2\pi}{x} \left[ \sum_{r=1}^{\infty} \frac{\coth(\pi x r) - 1}{r} + \ln r_{max} + C \right]. \quad (A6)$$

Employing the same techniques, we give the results of the different versions of Eq. (A5) below:

- 
- [1] I.F. Lyuksyutov and V.L. Pokrovsky, Adv. Phys. 54, 67 (2005).
- [2] S. Erdin, *Frontiers in Superconducting Materials*, edited by A. Narlikar, (Springer-Verlag, Berlin,2005),pp. 425-458.
- [3] I.F. Lyuksyutov and V.L. Pokrovsky, cond-mat/9903312 (unpublished).
- [4] I.F. Lyuksyutov and V.L. Pokrovsky, Modern. Phys. Lett. B **14**, 409 (2000).
- [5] S.Erdin, I.F. Lyuksyutov, V.L. Pokrovsky and V.M. Vinokur, Phys. Rev. Lett. **88**, 017001 (2002).
- [6] A.A. Abrikosov, *Introduction to the Theory of Metals* North Holland, (1986).
- [7] S. Erdin, A.M. Kayali, I.F. Lyuksyutov and V.L. Pokrovsky, Phys.Rev. B **66**, 014414 (2002).
- [8] S. Erdin, Physica C **391**,140 (2003).
- [9] M. Abramowitz and I. A. Stegun, *Handbook of Mathematical Functions*, (Dover Publications, New York, 1970).
- [10] S.Erdin, Phys.Rev.B **72**, 014522 (2005).
- [11] G.B. Arfken and H.J. Weber, *Mathematical Methods for Physicists*, (Academic Press, Orlando, 2000), 5th ed.
- [12] E.R. Hansen, *A Table of Series and Products*, (Prentice-Hall, Englewood Cliffs, 1975).